REPORT DOCUMENTATION PAGE

AFRL-SR-BL-TR-00-

86 68

1. AGENCY USE ONLY *(Leave blank)*	2. REPORT DATE	3. REPORT TYPE AND DATES COVERED
		Final Tech Report 31 Dec 95 TO 30 Jun 99

4. TITLE AND SUBTITLE
MODELING AND DESIGN FOR REDUCED CROSS TALK IN MIXED SIGNAL ANALOG/DIGITAL IC PACKAGES FOR WIRELESS APPLICATIONS

5. FUNDING NUMBERS
F49620-96-1-0032

6. AUTHOR(S)
D. P. Neikerk, Guanghan Xu, and Leszek Demkowicz

7. PERFORMING ORGANIZATION NAME(S) AND ADDRESS(ES)
Department of Electrical and Computer Engineering
University of Texas at Austin
Austin, TX 78712

8. PERFORMING ORGANIZATION REPORT NUMBER

9. SPONSORING/MONITORING AGENCY NAME(S) AND ADDRESS(ES)
Air Force Office of Scientific Research
AFOSR/NM
801 N. Randolph Street, Rm 732
Arlington, VA 22203-1977

10. SPONSORING/MONITORING AGENCY REPORT NUMBER
F49620-96-1-0032

11. SUPPLEMENTARY NOTES

20001208 045

12a. DISTRIBUTION AVAILABILITY STATEMENT
Approved for public release; distribution unlimited.

12b. DISTRIBUTION CODE

13. ABSTRACT *(Maximum 200 words)*

A critical requirement for the development of low cost, wide-bandwidth telecommunications equipment is the close integration of both digital and analog microelectronic components. The physical interface between an IC and its environment is the IC package, and its performance is severely tested by the high speed and high frequencies encountered in wide-bandwidth systems. Single chip mixed signal ICs that combine directly both high frequency analog and high speed digital sub-sections will require proper electromagnetic understanding of capacitive, inductive, and radiative coupling between components, and their impact on high sensitivity analog sub-circuits. The overall objective of this work is the development of techniques for the analysis and design of mixed signal packages, especially the impact of inductive cross talk between the digital and analog sections of the IC, and techniques to maintain appropriate RF to RF signal line isolation in low cost IC packages. In wireless personal communication services (PCS) units there are particularly severe constraints on package options, since these applications are typically very cost and form-factor sensitive. Some of the major problems induced by digital to analog and analog to analog cross talk are listed below: (1) high speed digital clocks cause severe interference with RF or IF front ends; (2) in digital portables, time-division- multiple-access (TDMA) may be used and power on / off cycles happen fairly frequently, causing additional transient noise on the power and ground planes; (3) in frequency division duplex systems, high-power transmit signals cause interference with weak receive signals since separation by filters is limited; (4) the leakage of the amplifier output to the input may cause the amplifier to oscillate.

14. SUBJECT TERMS	15. NUMBER OF PAGES
	31
	16. PRICE CODE

17. SECURITY CLASSIFICATION OF REPORT	18. SECURITY CLASSIFICATION OF THIS PAGE	19. SECURITY CLASSIFICATION OF ABSTRACT	20. LIMITATION OF ABSTRACT
UNCLASSIFIED	UNCLASSIFIED	UNCLASSIFIED	UL

Final Report for:

MODELING AND DESIGN FOR REDUCED CROSS TALK IN MIXED SIGNAL ANALOG / DIGITAL IC PACKAGES FOR WIRELESS APPLICATIONS

D. P. Neikirk, Guanghan Xu, and Leszek Demkowicz

The University of Texas at Austin

AFOSR Grant No. F49620-96-1-0032

Grant Start Date: 12/31/95

Final Report

POC: Professor Dean P. Neikirk

Department of Electrical and Computer Engineering

The University of Texas at Austin, Austin, TX 78712

voice: 512-471-4669; FAX: 512-471-5445

e-mail: neikirk@mail.utexas.edu; WWW: http://weewave.mer.utexas.edu

Introduction and objectives

A critical requirement for the development of low cost, wide-bandwidth telecommunications equipment is the close integration of both digital and analog microelectronic components. The physical interface between an IC and its environment is the IC package, and its performance is severely tested by the high speed and high frequencies encountered in wide-bandwidth systems. Single chip mixed signal ICs that combine directly both high frequency analog and high speed digital sub-sections will require proper electromagnetic understanding of capacitive, inductive, and radiative coupling between components, and their impact on high sensitivity analog sub-circuits.

The overall objective of this work is the development of techniques for the analysis and design of mixed signal packages, especially the impact of inductive cross talk between the digital and analog sections of the IC, and techniques to maintain appropriate RF to RF signal line isolation in low cost IC packages. In wireless personal communication services (PCS) units there are particularly severe constraints on package options, since these applications are typically very cost and form-factor sensitive. Some of the major problems induced by digital to analog and analog to analog cross talk are listed below:

(1) high speed digital clocks cause severe interference with RF or IF front ends;
(2) in digital portables, time-division-multiple-access (TDMA) may be used and power on / off cycles happen fairly frequently, causing additional transient noise on the power and ground planes;
(3) in frequency division duplex systems, high-power transmit signals cause interference with weak receive signals since separation by filters is limited;
(4) the leakage of the amplifier output to the input may cause the amplifier to oscillate.

Under this program, we are developing and testing electromagnetic modeling techniques that can capture such effects; to achieve this it is critical that the electromagnetic analysis tools exclude unnecessary effects, but without requiring "expert" intervention. We are developing inductive extraction processes that use ultra-compact equivalent circuits (consisting of frequency-independent elements) to model frequency dependent skin and proximity effects. Recent accomplishments include a new highly efficient simulation method, the surface ribbon method (SRM), that allows much more rapid simulation to be performed. Typically, computation time can be reduced by about a factor of 2000 compared the conventional model. We are currently preparing user software for transmission line impedance modeling based on the SRM, and expect release in first quarter 1997. We have recently derived a rigorous definition for the "effective internal impedance" used with the surface ribbon method, and will begin investigating its use with the finite element method. This approach should allow significant improvement in computation time for FEM-based electromagnetic simulations of finite conductivity structures. We are also studying internal-to-the-package low pass filter designs for analog power supply to chip; pad / pin arrangements for reduced digital power plane-to-analog coupling, for RF controlled impedance connections, and for increased RF-to-RF signal line isolation. Prototypical wireless communications circuits will be used to determine the impact of digital-to analog interference, and validate the models developed.

ACCOMPLISHMENTS

EFFECTIVE INTERNAL IMPEDANCE BOUNDARY CONDITION FOR FINITE CONDUCTIVTY METALS

Impedance boundary conditions (IBCs) are widely used in scattering problems, eddy current problems, and lossy transmission line problems. An IBC is usually adopted to simplify the problems by eliminating from the domain to be solved, for example, lossy dielectrics, multi-layered coatings on conductors in scattering problems, or the lossy conductors in eddy current and transmission line problems. Solutions can then be obtained by applying the finite element method (FEM) [1, 2], the boundary element method (BEM) [3, 4], the electric/magnetic field integral method (MFIE/EFIE) [5, 6], the finite difference time domain method (FDTD) [7, 8], etc.. In each case, the use of an IBC reduces the number of unknowns and can substantially reduce the computation time required. But, in general, the boundary condition must be known (at least approximately) *a priori* on the surface, and the accuracy of the field solution is determined by the accuracy with which the IBC is approximated.

The most widely used IBC is the standard impedance boundary condition (SIBC), also called the Leontovich boundary condition [9, 10], that was originally developed for use when the skin depth is small relative to other dimensions of the problem, or a layer is thin and highly lossy. In general, for coated dielectric layers on scatterers, the reflection of the electromagnetic wave at the boundary depends on the angle of the incident wave, and hence requires higher level of IBCs [10], such as the Tensor Impedance Boundary Condition (TIBC), the Higher Order Impedance Boundary Conditions (HOIBC), etc. For eddy current and transmission line problems, the Leontovich boundary condition has been used to model lossy conductors at high frequency. In this paper, an efficient approach for calculating the series impedance of lossy multi-conductor lines from DC to high frequency is presented that use the effective internal impedance (EII) as an impedance boundary condition. The advantage of the EII when compared to the SIBC is that even for strongly coupled transmission lines it is easily approximated from low frequency (i.e., the skin depth is larger than the cross-sectional dimensions of the conductors) to high frequency (i.e., the skin depth is far smaller than the dimensions of the conductors) using the surface impedance of an isolated conductor. As an example, the EII-based method and the SIBC combined with the BEM are compared in the case of twin lead conductors, and the appropriateness of the EII approach is shown for series impedance calculations of lossy quasi-TEM transmission lines from DC to high frequency.

Schelkunoff [11] first introduced the concept of surface impedance in electromagnetics in 1934 for the analysis of coaxial cables. In the 1940's Leontovich [9] as well as many other workers studied the basic properties of the surface impedance for a semi-infinite plane of an isotropic linear medium and on a conductor-backed thin lossy dielectric layer where a plane wave is incident. Senior [12] explained in detail the Leontovich boundary conditions and the requisites to be satisfied.

In order to approximate the SIBC for multi-conductor problems the relationship between the tangential electric and magnetic fields at any point on the boundary must be (at least approximately) a local one, depending only on the curvature of the surface and the local electromagnetic properties (i.e., μ, ε, and σ) of the bodies. Hence the surface impedance must not be altered by the global geometry of the conductor or the existence of other conductors in a problem. This constraint will hold if the operating frequency is "high" (but much lower than the dielectric relaxation frequency), i.e., when the curvature radius of the surface is larger than the skin depth, when the refractive index of the bodies is larger than that of the external medium, and

when the dimensions of the problem are smaller than the wavelength. In such circumstances, the reflection characteristic is independent of the incident angle. For geometries having curvature, Leontovich introduced a first order curvature correction term to the surface impedance for small radii of curvature and Mitzner [13] later refined this.

At low and middle frequency where the skin depth is comparable to or larger than the dimensions of the conductors, the surface impedance is strictly no longer a local property and depends on the global geometries of the conductors. For "thin-film" transmission lines using metals with thicknesses of less than a few micrometers, such a condition may hold for frequencies well into the GHz range. Under such conditions the surface impedance when other conductors are present may considerably differ from the surface impedance of an isolated conductor. Hence, it is difficult to know or approximate *a priori* the surface impedance in lossy multi-conductor systems at low to middle frequencies. This limits the usefulness of the SIBC for calculating the series impedance of lossy quasi-TEM transmission lines at low and middle frequencies, and necessitates complicated models for the IBC.

It would be useful to find some technique in which surface characteristics can be more easily approximated than the standard surface impedance boundary condition. Instead of developing complicated SIBC models to capture the coupling and non-localized field effects between multiple conductors at low and middle frequency it is possible to develop a formulation in which *isolated* conductor surface impedance is a useful approximation. In this approach, the conductor interior is not excluded from the domain of solution, but rather the conductor interior is replaced by the exterior medium and the Green's function of the exterior medium is used also for the interior region in the equivalent problem. The conductor is now modeled as an impedance sheet at the conductor surface, as shown in Fig. 1b.

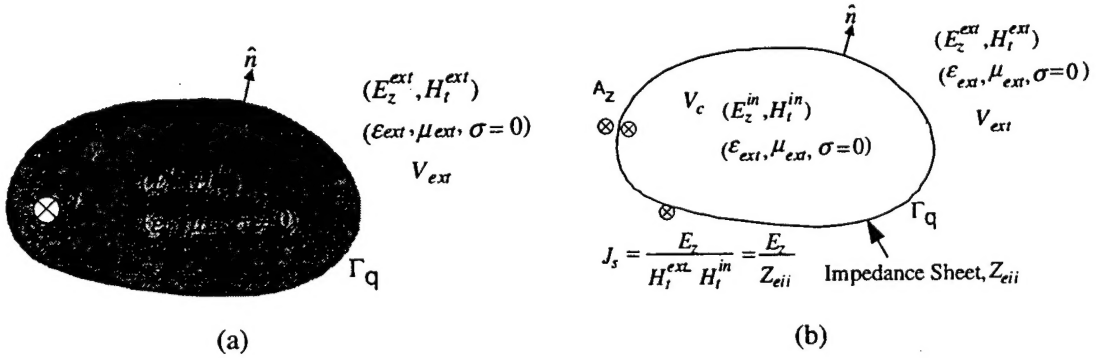

Figure 1: Comparison of the actual geometry and various surface equivalent models.
(a) actual geometry with the descriptions of fields and material properties; (b) the equivalent model using the effective internal impedance (EII) where the exterior fields are identical to the original problem, the conductor interior is replaced by the exterior medium, and an impedance sheet is defined at the conductor surface.

The volume filament technique (Figure 2a) has been widely used in high performance package modeling since an external Green's function can be used to calculate mutual inductances between conductors regardless of their different conductivities, avoiding solving complicated boundary condition problems that are often encountered in surface equivalent problems. Also, this technique directly calculates resistances and inductances (rather than field quantities) that are

frequently required for circuit simulation. According to the equivalence theorem, the original problem can be replaced with equivalent surface currents as long as this current generates the correct fields outside of the conductors, while the fields inside of the conductor can be assumed to be arbitrary. This allows one to replace the medium inside the conductor boundaries with the same medium as the external region. Consequently, an external Green's function can be used everywhere in the integral equations.

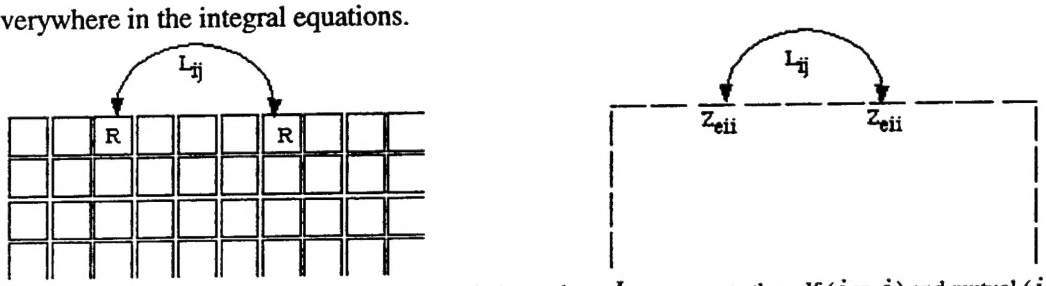

Figure 2: (a) Illustration of the volume filament technique where L_{ij} represents the self ($i = j$) and mutual ($i \neq j$) inductances between filaments; R is filament resistance given by $1/\sigma A$ where A is the cross-sectional area of the filament. (b) Surface ribbon method where L_{ij} represents the self and mutual inductance between surface ribbons and Z_{eii} is the diagonal elements of $[Z_{eii}]$ given in (16).

In formulating a surface boundary condition the fields inside of the conductor are usually assumed to be zero [16], but here we assume the vector magnetic potential is continuous across conductor surfaces, and the equivalent surface current is defined as the difference between original tangential magnetic field and internal tangential magnetic field generated in this new equivalent problem. Figure 1 shows the original problem and the equivalent problem explained here. Of course, it might seem that this new approach would make problem much more complicated, but as will be demonstrated in this paper, the surface impedance boundary condition satisfying this new problem, the effective internal impedance (EII), is much more localized than the SIBC from low to high frequencies.

The surface integral equation can be obtained from Green's theorem [3]

$$\iint ds'\left(\Phi\nabla^2\Psi - \Psi\nabla^2\Phi\right) = \oint dr'\left(\Phi\frac{\partial\Psi}{\partial n'} - \Psi\frac{\partial\Phi}{\partial n'}\right). \tag{1}$$

For the exterior region where Green's function satisfies $\nabla^2 G = -\delta(r-r')$ and magnetic vector potential satisfies Laplace's equation, $\nabla^2 A_z = 0$, the equation (1) becomes

$$\iint ds'[A_z(r')\delta(r-r')] = -\oint dr'\left[G(r,r')\frac{\partial A_z(r')}{\partial n'} - A_z(r')\frac{\partial G(r,r')}{\partial n'}\right], \tag{2}$$

where $\Psi = A_z$, $\Phi = G$, and negative sign in right side of (2) indicates derivative with respect to normal pointing inwards. Similarly, for the interior region where Green's function satisfies $\nabla^2 G - j\omega\mu\sigma G = -\delta(r-r')$ and longitudinal electrical current satisfies $\nabla^2 J_z - j\omega\mu\sigma J_z = 0$, the equation (1) becomes

$$\iint ds'[E_z(r')\delta(r-r')] = \oint dr'\left[G(r,r')\frac{\partial E_z(r')}{\partial n'} - E_z(r')\frac{\partial G(r,r')}{\partial n'}\right], \tag{3}$$

where $\Psi = J_z = \sigma E_z$ and $\Phi = G$.

The surface integral equation is formulated on the surface of the conductors, which requires appropriate distribution of the delta functions in the equations (2) and (3). Suppose that at given location the strength of the delta function just outside of the surface is $p(r')$. Then the strength of the delta function just inside of the surface is $1-p(r')$. The left side of the equation (2) equals to $p(r)A_z(r)$, which can be expressed as $\oint dr'[p(r')A_z(r')\delta(r-r')]$. After applying $\nabla\times\vec{A}=\mu\vec{H}$, the surface integral equation for the exterior region becomes

$$\oint dr'\left[G^1_{ext}(r,r')\mu H_t(r')\right]-\oint dr'\left[G^2_{ext}(r,r')-p(r')\delta(r-r')\right]A_z(r')=0\ , \qquad (4)$$

where H_t and A_z are the tangential magnetic field and longitudinal magnetic vector potential respectively, $p(r')$ is the position dependent coefficient describing source strength distribution just outside of the conductor surface, and G^1_{ext} and G^2_{ext} are the free space external Green's function and its derivative with respect to the surface normal, respectively, and the integral is carried out along the perimeter of all conductors. Similarly, for the interior region, the left side of the equation (3) equals to $[1-p(r)]E_z(r)$, which can be expressed as $\oint_{\Gamma_q}\{[1-p(r')]E_z(r')\delta(r-r')\}$. After applying $\nabla\times\vec{E}=-j\omega\mu\vec{H}$, the integral equation for the inner region becomes

$$\oint_{\Gamma_q} dr'\left[G^1_q(r,r')j\omega\mu H_t(r')\right]+\oint_{\Gamma_q} dr'\left[G^2_q(r,r')+[1-p(r')]\delta(r-r')\right]E_z(r')=0\ , \qquad (5)$$

where G^1_q and G^2_q are the Green's function and its normal derivative for conductor q respectively, and the integral is carried out along the each individual conductor perimeter Γ_q. Equation (4) and (5) should satisfy

$$\oint_{\Gamma_q} dr' H_t = I_q\ , \qquad (6)$$

where I_q is the total current carried by conductor q.

After applying the equivalence theorem, the Green's function that appears in equation (5) can be replaced by the free space Green's function used in (4). In this paper we use continuity of the vector magnetic potential across conductor surfaces to complete the definition of the EII. Equation (4) for the exterior region becomes

$$\oint dr'\left[G^1_{ext}(r,r')\mu H_t^{ext}(r')\right]-\oint dr'\left[G^2_{ext}(r,r')-p(r')\delta(r-r')\right]A_z(r')=0\ , \qquad (7)$$

where H_t^{ext} is the external tangential magnetic field. For the interior region where internal medium is replaced with external medium equation (5) becomes

$$\oint dr'\left[G^1_{ext}(r,r')\mu H_t^{in}(r')\right]-\oint dr'\left[G^2_{ext}(r,r')+[1-p(r')]\delta(r-r')\right]A_z(r')=0\ , \qquad (8)$$

where H_t^{in} is the internal tangential magnetic field and the integral is now carried out along the entire surface of inside of the conductor.

If the values of external tangential magnetic field and magnetic vector potential are exactly known in equation (7) (here, magnetic vector potential is related to magnetic field by

$\vec{B} = \nabla \times \vec{A}$), the position dependent coefficient $p(r')$ can be determined, and then H_t^{in} can be found from equation (8).

For this new equivalent problem, the relationship between the longitudinal electric field and the difference of the tangential magnetic fields across the equivalent surface impedance sheet is called the effective internal impedance (the EII, to distinguish it from the SIBC), and is then

$$Z_{eii}(\omega, r') = \frac{|E_z(r')|}{|H_t^{ext}(r') - H_t^{in}(r')|} = \frac{|E_z(r')|}{|J_s(r')|} \quad , \tag{9}$$

where Z_{eii} is the EII and J_s is the equivalent surface current density.

To compute the integrated quantities of series impedance using the EII approach, power applied, power dissipated, and magnetic energy stored in the equivalent problem are found using

$$-\int_S ds \nabla \Phi^q \cdot \vec{J}_s^* = \int_S ds Z_{eii} |J_s|^2 + j\omega \int_S ds \vec{A} \cdot \vec{J}_s^* \quad , \tag{10}$$

where S is the conductor surface and Φ is the electric potential. The left-hand side of the equation (10) is the power applied, the first term of right-hand side is the power dissipated, and the second term corresponds to the magnetic energy stored. From the power dissipation term in (10), resistance can be calculated using

$$R_q^{srm}(\omega) = \frac{\oint_{\Gamma_q} dr' \mathrm{Re}\left\{ Z_{eii} |J_s|^2 \right\}}{\left| \oint_{\Gamma_q} dr' J_s \right|^2} \cdot l_q \quad , \tag{11}$$

where l_q is the length of the line q. Internal inductance of conductor q and total external inductance are calculated from the stored magnetic energy term,

$$L_{in,q}^{srm}(\omega) = \frac{\mu \int_{V_q} dv \vec{H}^{in} \cdot \vec{H}^{in*}}{|I_q|^2} = -\frac{\int_{S_q} ds \hat{n} \cdot \left(\vec{A} \times \vec{H}^{in*} \right)}{\left| \oint_{\Gamma_q} dr' J_s \right|^2}$$

$$= -\frac{\oint_{\Gamma_q} dr' \mathrm{Im}\left\{ E_z H_t^{in*} \right\}}{\omega \left| \oint_{\Gamma_q} dr' J_s \right|^2} \cdot l_q \tag{12}$$

and

$$L_{ext}^{srm}(\omega) = \frac{\mu \int_{V_{ext}} dv \vec{H}^{ext} \cdot \vec{H}^{ext*}}{\sum_{q=1}^{m} |I_q|^2} = \frac{\int_S ds \hat{n} \cdot \left(\vec{A} \times \vec{H}^{ext*} \right)}{\sum_{q=1}^{m} \left| \oint_{\Gamma_q} dr' J_s \right|^2}$$

$$= \sum_{q=1}^{m} \left(\frac{\oint_{\Gamma_q} dr' \mathrm{Im}\{E_z H_t^{ext*}\}}{\omega \left| \oint_{\Gamma_q} dr' J_s \right|^2} \right) \cdot l_q \quad , \tag{13}$$

where V_{ext} is the volume exterior to the conductors. The surface inductance due to the magnetic energy stored by the impedance sheet is given by

$$L_{sur,q}^{srm}(\omega) = \frac{\int_S ds \, \mathrm{Im}\{Z_{eii}^q |J_s|^2\}}{\omega |I_q|^2} = \frac{\oint_{\Gamma_q} dr' \mathrm{Im}\{Z_{eii}^q |J_s|^2\}}{\omega \left| \oint_{\Gamma_q} dr' J_s \right|^2} \cdot l_q \quad . \tag{14}$$

Finally, the sum of internal, external, and surface inductances from (12), (13), and (14) gives the total series inductance for the transmission line in the EII formulation.

To validate equations (11) to (14), a similar procedure can be used to derive the equations for series impedance using the boundary element method [3, 17]. Using the exact exterior magnetic and electric fields from the original problem, it can be shown that the resistances given by (11) are identical to the original problem, that the external inductance given by (13) is identical to the original problem, and the sum of (12) and (14) is identical to the internal inductances in the original problem.

III. Surface Ribbon Method

For series impedance calculation, even though (11) to (14) are useful to validate the new approach, it is a time-consuming task to solve the coupled integral equations. A much simplified formulation can be derived directly from (7), (8), and (9) on the surface of the conductor. By subtracting (8) from (7) and applying (9) and $E_z + \nabla_z \Phi = -j\omega A_z$ at the boundary of the conductors, the following integral equation results for m conductor system.

$$\sum_{q=1}^{m} \oint_{\Gamma_q} dr' \{ j\omega\mu G_{ext}^1 + \delta(r-r') Z_{eii}(r') \} J_s(r') + \sum_{q=1}^{m} \oint_{\Gamma_q} dr' \delta(r-r') \nabla_z \Phi^q = 0 \quad . \tag{15}$$

Each conductor perimeter Γ_q can be further divided into N_q segments, each with sub section $C_{q,k}$, where these pieces represent current-carrying "ribbons" of width $w_{q,k} = \int_{C_{q,k}} dr$. Equation (15) then becomes

$$Z_{eii}^{q,k}(r) J_s^{q,k}(r) + j\omega\mu \sum_{i=1}^{m} \sum_{j=1}^{N_i} \int_{C_{i,j}} dr' J_s^{i,j}(r') G_{ext}^1(r,r') = -\nabla_z \Phi^{q,k} \, , \tag{16}$$

where $Z_{eii}^{q,k}$ and $J_s^{q,k}$ are respectively, the effective internal impedance and sheet current density on the kth ribbon ($k = 1,2,\cdots,N_q$) of the qth conductor ($q = 1,2,\ldots,m$) at a given frequency, and the second term on the left hand side represents contributions from self and mutual inductances. For a two dimensional case $G_{ext}^1(r,r') = -\frac{1}{2\pi} \ln|r-r'|$. If the ribbons are narrow enough that the sheet current density is constant across each ribbon, integrating over the kth ribbon yields

$$\frac{I_s^k}{w_k}\int_{C_k} drZ_{eii}^k(r)+j\omega\mu\sum_{i=1}^{N}\frac{I_s^i}{w_i}\int_{C_k}\int_{C_i} dr'drG_{ext}^1(r,r')=-\int_{C_k} dr\nabla_z\Phi^k \quad , \tag{17}$$

where I_s^k is the total sheet current carried by the k[th] ribbon, and for simplicity the double superscript (q,k) has been replaced with the single superscript k $(k=1,2,\ldots,N,\ N=N_q\times m)$. Finally,

$$\overline{Z_{eii}^k}I_s^k\frac{l_k}{w_k}+j\omega\mu\sum_{i=1}^{N}\frac{I_s^i l_k}{w_k w_i}\int_{C_k}\int_{C_i} dr'drG_{ext}^1(r,r')=\Phi_1^k-\Phi_2^k \quad , \tag{18}$$

where $\Phi_1^k-\Phi_2^k$ is voltage drop along the ribbon k, $\overline{Z_{eii}^k}$ is the EII averaged over the width of ribbon k, and l_k is the length of ribbon k, which is assumed to be 1 in a two dimensional problem. Equation (18) can be expressed as an N x N matrix equation

$$[([Z_{eii}]+j\omega[L])][I]=[V] \tag{19}$$

where $[Z_{eii}]$ is an N x N diagonal matrix made up of the $\overline{Z_{eii}^k}/w_k$ and $[L]$ is a matrix consisting of self and mutual inductances between surface ribbons. This approach is called the surface ribbon method (SRM). Now rather than calculating resistance and inductance from equation (11) to (14), if $[Z_{eii}]$ is known (19) can be used to calculate resistance and inductance directly, as is done in the volume filament method [1, 2]. As shown in the following section, the EII has relatively localized characteristics, allowing $[Z_{eii}]$ to be easily approximated.

Just as in the SBEM, in principle it is as difficult to find *a priori* the exact EII, especially at low and middle frequencies, as solving the original problem. However, it will be shown below that the surface impedance of a single, isolated conductor is a better approximation to the EII than to the SIBC for multi-conductor transmission lines at low frequencies, while at high frequencies the isolated conductor surface impedance is an adequate approximation of both the EII and the SIBC. Hence, more accurate approximation of the transmission line series impedance can be obtained over a wider frequency range using the more easily calculated isolated conductor surface impedance as an EII in the SRM than can be achieved using the same isolated surface impedance as the SIBC in, for instance, the SBEM.

IV. Sample Results

To calculate the exact EII, the volume filament technique can be used to find the external magnetic and electric fields and the vector magnetic potential, then these values can be used in (7) and (8) to calculate the internal magnetic field, and finally the EII is found using (9). Fig. 3 shows a comparison between the EII values for two circular conductors with radii 1 mm separated by 0.2 mm, 20 mm, and 200 mm, and the surface impedance of an isolated circular conductor given by [18],

$$Z_{cir}=\frac{j\sqrt{j\omega\mu\sigma}}{\sigma}\frac{J_0\left(ja\sqrt{j\omega\mu\sigma}\right)}{J_1\left(ja\sqrt{j\omega\mu\sigma}\right)} \quad , \tag{20}$$

where a is the radius of the conductor. The most interesting characteristics of the EII is the position independence of the real part at low frequency, as shown in Fig. 3a. All real parts of the

EII are almost constant and are quite close to the surface impedance of the isolated conductor calculated from (20). The imaginary parts do have a position dependence, especially when two conductors are very close to each other. However, this dependence diminishes quickly as the two conductors are separated, with values of Im(EII) being approximately the average of that obtained from (20). At high frequency, the internal fields of the conductors approach zero, and the EII calculated from (9) is expected to approach to the SIBC which is accurately approximated by (20) in the high frequency limit. Fig. 3b shows that this does indeed occur. In other words, (20) can be used as an approximation of the EII to calculate series impedance of circular conductors regardless of the frequency or proximity of other conductors (i.e., $\overline{Z_{eii}^{k}} \approx Z_{cir}$ in (18) and (19)). To support this point, the series impedance of two circular conductors separated by 0.2 mm is calculated and compared with the volume filament method as shown in Fig. 4. Here, a polygon with degree 24 shown in Fig. 4a is used instead of a circular conductor to simplify the calculation of the mutual inductance between ribbons. Figure 4b indicates (20) is indeed a good approximation of the EII for series impedance calculation even when conductors are very close to each other.

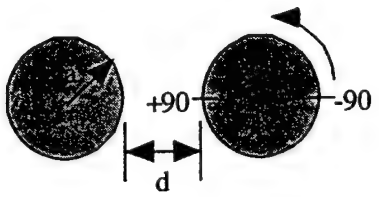

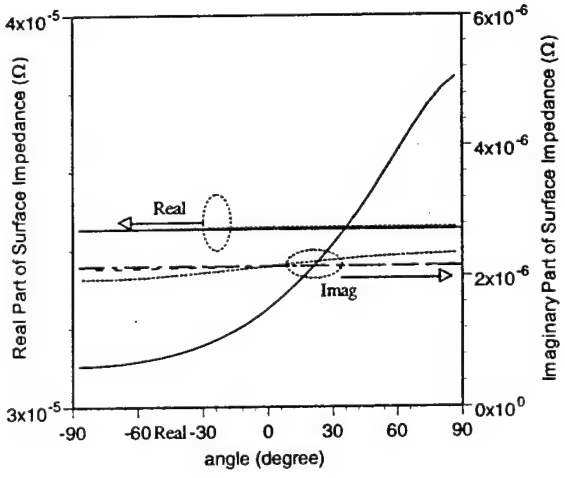

Figure 3(a)

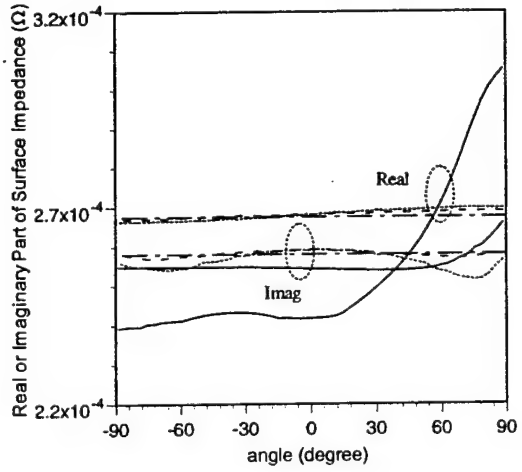

Figure 3(b)

Figure 3: Position dependency of EII for circular conductor (copper) with a = 1mm, d = 0.2, 20, and 200 mm. solid line: d = 0.2 mm, dotted line: d = 2 mm, dashed line: d = 200 mm, dot-dash line: equation (17). (a): low frequency limit (1 kHz); (b): high frequency limit (1 MHz).

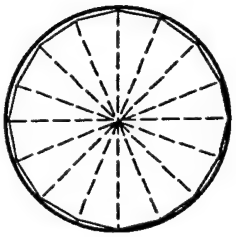

Figure 4(a)

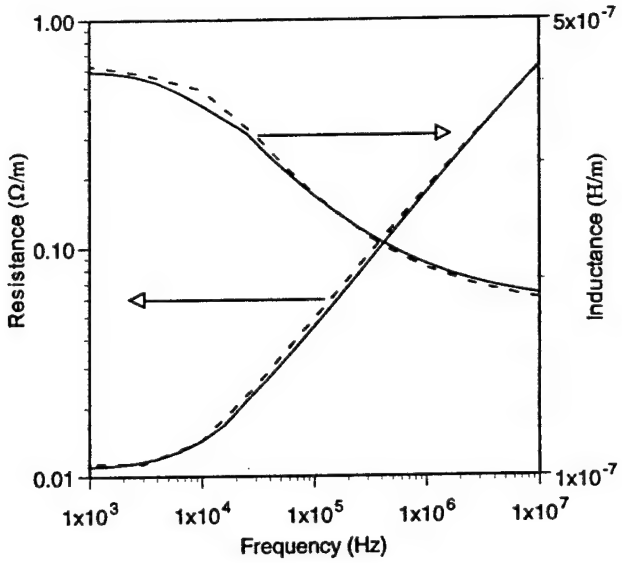

Figure 4(b)

Figure 4: (a) Segmentation scheme for circular conductor using polygon of degree 24 in the SRM. (b) Series impedance calculation of two closely spaced circular conductors (copper) with a = 1 mm, d = 0.2 mm, N = 48. Solid line: SRM; dashed line: VFM

The EII values for square conductors with width 25 μm and separated by 5 μm and 50 μm have also been calculated. It is impossible to calculate exactly the SIBC of isolated square or rectangular conductors due to the singularity at the corner, however, it can be approximated [19-21]. Fig. 5 shows the low frequency characteristics of the EII. Both real and imaginary parts of the EII show similar characteristics as the circular case except near the corner.

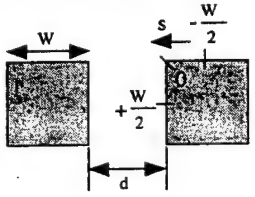

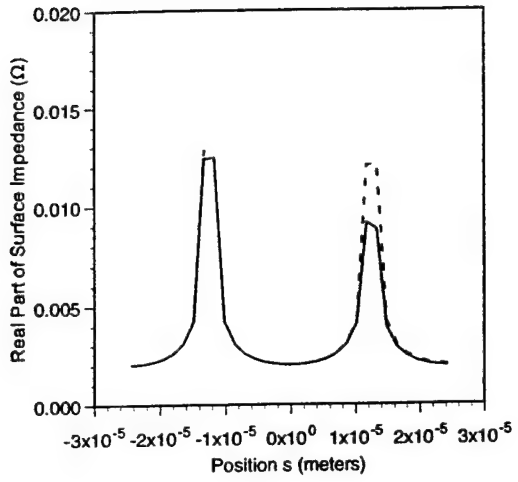

Figure 5(a)

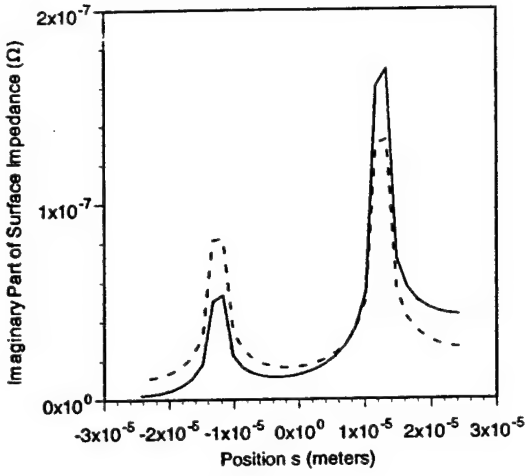

Figure 5(b)

Figure 5: Position dependency of EII for square conductor (copper) with 25 μm width and d = 5 μm and 50 μm at f = 1kHz. solid line: d = 5 μm, dashed line: d = 50 μm. (a) real part (b) imaginary part.

At high frequency, the surface impedance of an infinitely wide and thick conductor given by

$$Z_s = \sqrt{\frac{\pi f \mu}{\sigma}}(1+j) \qquad (21)$$

is a reasonable approximation for the SIBC far from corners; Fig. 6 shows that the EII also approaches (21) except near the corner. Examination of other geometrical cases has confirmed that the EII is well approximated by the surface impedance of an isolated conductor, regardless of the presence of other conductors. Various studies [17, 22] have shown that an approximated EII can be directly applied to (19) to accurately estimate the series impedance of various cross-sectional conductors. The series impedance calculations for multi-conductor transmission lines using the SRM are detailed in [17, 22].

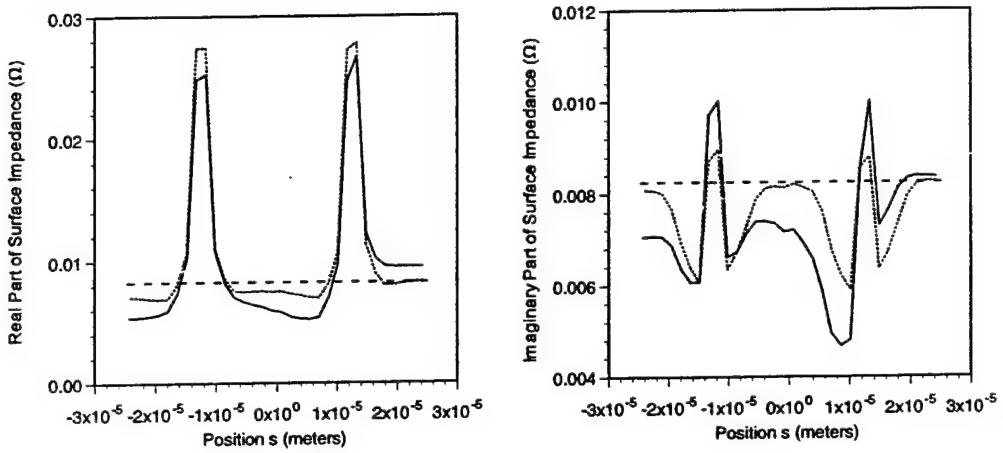

(a) (b)

Figure 6: Position dependency of EII for square conductor (copper) with 25 μm width and d = 5 μm and 50 μm at f = 1 GHz. solid line: d = 5 μm, dotted line: d = 50 μm, dashed line: equation (18). (a) real part (b) imaginary part.

V. Conclusions

The precise definition of an alternative surface impedance boundary condition has been formulated for use in lossy transmission line analysis. For this boundary condition, the conductor is modeled as an impedance sheet on the conductor perimeter, the conductor interior is replaced by a (non-conducting) exterior material, and the effective internal impedance (EII) is defined on the impedance sheet. At low frequency, the real part of the EII is almost constant along the perimeter of a conductor, and at high frequency the EII approaches the SIBC; hence, the EII is approximately a local quantity from low to high frequency. Approximations to the EII can be used in the surface ribbon method, producing numerically efficient and accurate calculation of the series impedance of lossy multi-conductor lines. Here, the SRM was applied to two dimensional problems, but can be extended to three dimensional problems [17]. Since this method requires substantially less memory than the VFM, the SRM can be used effectively for ground plane modeling including current crowding effects.

Table 1 compares the number of unknowns and run time on an IBM RISC 6000 for the FBEM, the I-BEM, and the I-SRM. The surface techniques are at least 25 times faster than the FBEM in assembling the required matrices, and at least 11 times faster in solving using a gaussian elimination algorithm. In addition, the SRM and the SBEM require matrix assembly only once for all frequencies of interest, while FBEM requires assembling the matrix at each frequency. Hence, the surface techniques are significantly more computationally efficient, and by using the isolated conductor surface impedance as an approximation for the EII in the SRM, little accuracy is lost over the whole low-to-high frequency range.

Method	Number of unknowns	CPU time (sec) Assembling	Solving
BEM	578	468.1	100.10
I-SBEM	290	18.3	8.05
I-SRM	287	5.1	8.96

Table 1: Run time comparison between BEM and SRM.
Comparison of run time on an IBM RISC 6000 for BEM, BEM assuming the SIBC is equal to the isolated conductor surface impedance (I-SBEM), and SRM assuming the EII is equal to the isolated conductor surface impedance (I-SRM). The surface of a conductor is segmented into 144 elements. I-SBEM and I-SRM are at least 25 times faster than BEM in assembling a matrix, and at least 11 times in solving the matrix using a simple gaussian elimination algorithm.

In summary, this work has shown a new surface impedance technique that can be accurately approximated using the isolated conductor surface impedance, even at low frequency. This effective internal impedance (EII) can be combined with the surface ribbon method (SRM) allowing numerically efficient and accurate calculation of the series impedance of lossy multi-conductor transmission lines. In this technique, the effective internal impedance defines an impedance sheet at the conductor surfaces and the conductor interiors are replaced with the exterior dielectric. For circular cross section conductors, using the surface impedance of an isolated circular conductor in the EII-based SRM yields an excellent approximation from low to high frequency. This technique can also be easily applied to any lossy multi-conductor line structure using polygonal cross-section conductors by using an appropriate effective internal impedance model.

SIMIAN: A TWO DIMENSIONAL MULTI-CONDUCTOR INTERCONNECT SERIES IMPEDANCE CALCULATOR

SIMIAN (Surface Impedance Method for Interconnect Analysis) is a two dimensional frequency dependent series impedance extraction tool for interconnects and transmission lines using conductors of rectangular cross section based on the EII and SRM discussed above. Unlike the Volume Filament Method [19], only the surface of the conductor is divided, which can save significant amounts of computation time, especially when the cross sectional size of the conductor(s) is (are) comparable to the skin depth [14]. This method has also been extended to solve three dimensional problems [15]. SIMIAN returns the frequency dependent series impedance matrix for an n-conductor system, i.e., the n x n matrix consisting of self and mutual resistances and self and mutual inductances of and between all n conductors.

The SIMIAN program was successfully complied with ANSI C(g++). The platforms tested thus far include:

- Sparc 20 machine with Sunos 4.1.3
- Sparc 20 machine with Solaris 2.5
- Pentium machine with Linux
- HP workstation

The progran can be obtained over the World Wide Web at the url:

http://weewave.mer.utexas.edu/MED_files/MED_research/Intrcncts/SIMIAN_stuff/simian_links.html

Since the total number of ribbons used for each conductor determines the computation time, it is very important to reduce them without loss of accuracy. Since SIMIAN only divides the conductor on its surface, the problem can be reduced from N^2 to 4N compared to the volume filament method. However, more significant advantage comes from reduction of N itself. To get accurate result in the volume filament method, each segment has to be comparable in size to the skin depth at the frequency of interest; if a filament is much larger than about 1/3 of a skin depth, serious error can result. However, in the surface ribbon method a much smaller number of segments can be used while maintaining reasonable accuracy (typically less than 1% error at "low" frequencies, perhaps as much as 10% over a narrow band of frequencies at "mid" frequency, and again about 1% at "high" frequency). For most cases using more than five ribbons on each side would not be necessary, and in many cases as few as one per face is necessary.

Figure 7 shows minimum segmentation method [20] using '**plate**' option in Conductor type variable applied to ground plane. Only one ribbon is used on each side of signal line resulting in a total of 20 ribbons.

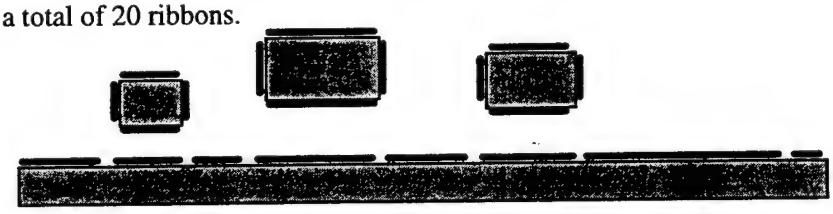

Figure 7: Minimum Segmentation Scheme with ground plane.

Examples and Results

Square Twin Lead

Example 1 is simulated with SIMIAN and compared with FastHenry [21] that uses the volume filament method accelerated using a multi-pole algorithm. As Fig. 8 shows, SIMIAN can reduce matrix size significantly. For the problem given, SIMIAN only uses 30 to 40 total ribbons while the volume filament method needs more than 800 filaments to accurately predict total resistance at high frequency. FastHenry accelerates matrix calculation with the help of a multi-pole algorithm, and this same algorithm can also be applied to the surface ribbon method. Figure 9 shows the results of FastHenry, SIMIAN, and the surface ribbon method (SRM) using a multi-pole algorithm. A total 40 ribbons were used for SIMIAN and SRM with multi-pole algorithm, while 800 filaments were used for FastHenry. In this particular example, the time advantage can be 400 to 8000 times faster than using the volume filament method, depending on what method is used for matrix calculation. Considering this is for only one frequency point, tremendous time savings can be achieved by using the SRM.

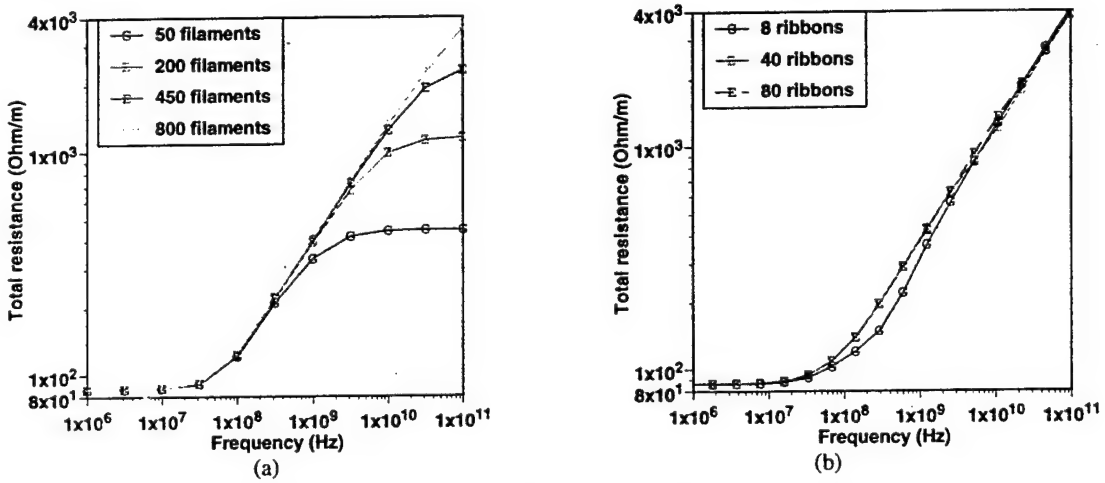

Figure 8: (a) FastHenry [21] results versus number of filaments; (b) SIMIAN versus number of ribbons.

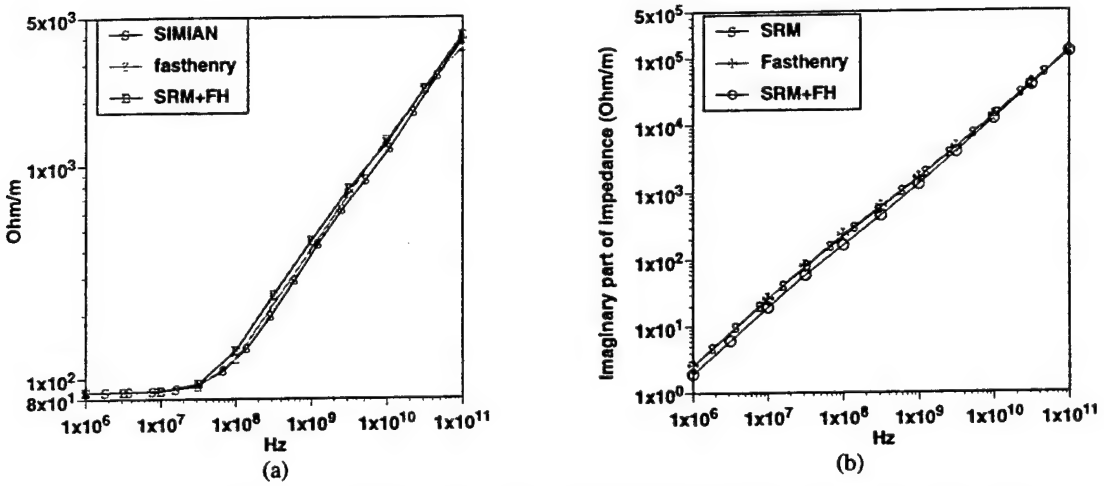

Figure 9: solid line: SIMIAN (40 ribbons); circle: SRM with multi-pole algorithm (40 ribbons); cross: FastHenry (800 filaments). (a) Real part of total Impedance (R). (b) Imaginary part of total Impedance (ωL).

Three Conductors over Finite Size/Conductivity Ground Plane

Figure 10 shows results from simulating the three conductor problem shown below. The total number of ribbons used in SIMIAN was 20, which was considerably less than FastHenry (1250). Reasonable accuracy was achieved through SIMIAN within a second (20 frequency points with SPARC 20).

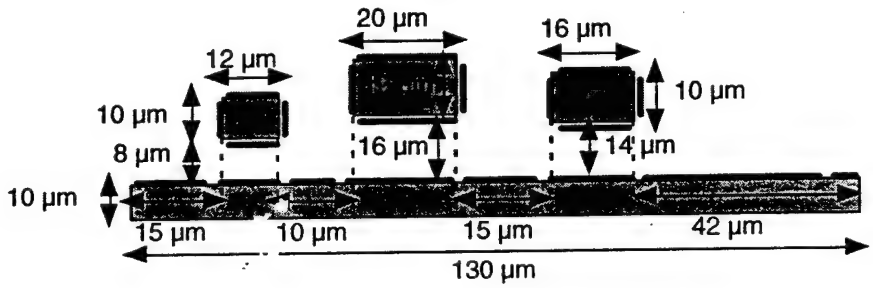

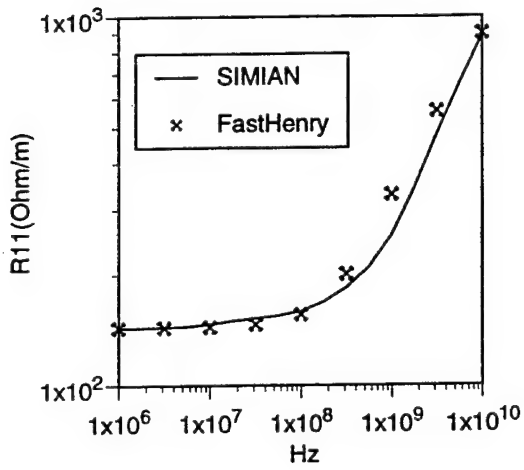

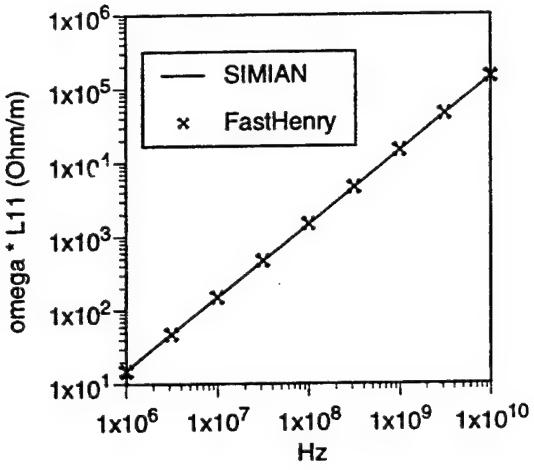

(a)Example 2, Z11

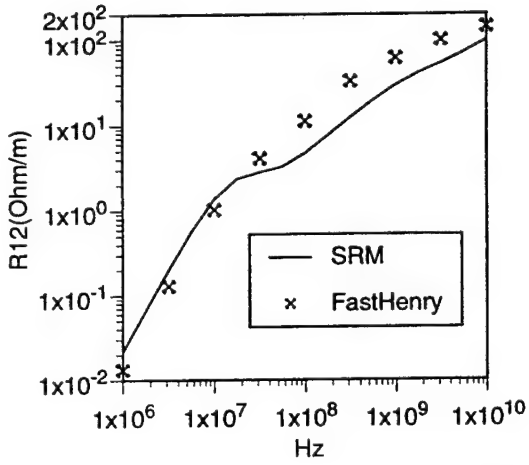

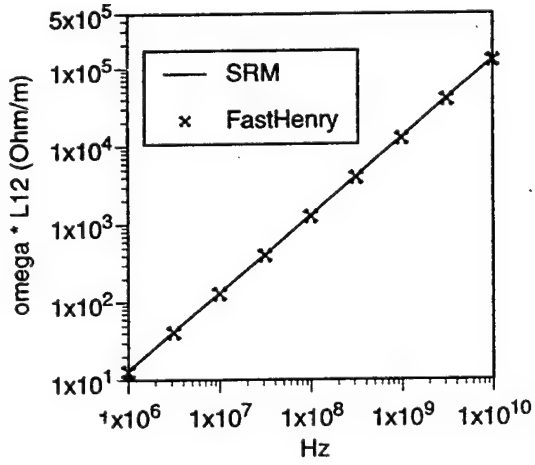

(b)Example 2, Z12

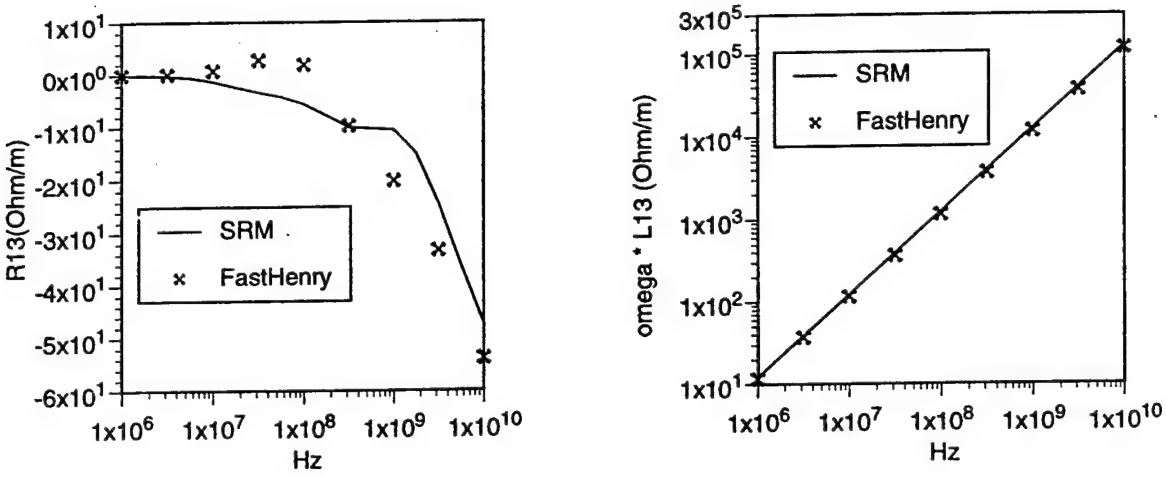

(c)Example 2, Z13

Figure 10: Real and Imaginary part of Series Impedance of Example 2.

REFERENCES

[1] J. Jin, *The Finite Element Method in Electromagnetics*: John Wiley & Sons, Inc., 1993.

[2] A. Darcherif, A. Raizer, J. Sakellaris, and G. Meunier, "On the use of the surface impedance boundary concept in shielded and multiconductor cable characterization by the finite element method," *IEEE Trans. Magnetics*, vol. 28, pp. 1446-1449, 1992.

[3] T. H. Fawzi, M. T. Ahmed, and P. E. Burke, "On the use of impedance boundary conditions in eddy current problems," *IEEE Trans. Magnetics*, vol. MAG-21, pp. 1835-1840, 1985.

[4] E. M. Deely, "Avoiding surface impedance modification in BE methods by singularity-free representations," *IEEE Trans. Magnetics*, vol. 28, pp. 2814-1816, 1992.

[5] J. R. Mosig, "Arbitrary shaped microstrip structures and their analysis with a mixed potential integral equation," *IEEE Trans. Microwave Theory Tech.*, vol. 36, pp. 314-323, 1988.

[6] B. J. Rubin, "An electromagnetic approach for modeling high-performance computer packages," *IBM J. Res. Develop.*, vol. 34, pp. 585-600, 1990.

[7] J. G. Maloney and G. S. Smith, "The use of surface impedance concepts in the finite-difference time-domain method," *IEEE Trans. Antennas Prop.*, vol. 40, pp. 39-48, 1992.

[8] J. H. Beggs, R. J. Luebbers, K. S. Yee, and K. S. Kunz, "Finite-difference time-domain implementation of surface boundary conditions," *IEEE Trans. Antennas Prop.*, vol. 40, pp. 49-56, 1992.

[9] M. A. Leontovich, "On the approximate boundary conditions for electromagnetic fields on the surface of well conducting bodies," *Investigations of Propagation of Radio Waves*, vol. B. A. Vvdensky, Ed. Moscow: Academy of Sciences USSR, pp. 5-20, 1948.

[10] D. J. Hoppe and Y. Rahmat-Samii, *Impedance Boundary Conditions in Electromagnetics*: A SUMMA Book, 1995.

[11] S. A. Schelkunoff, "The electromagnetic theory of coaxial transmission lines and cylindrical shields," *Bell System Technical Journal*, vol. 13, pp. 532-579, 1934.

[12] T. B. Senior, "Impedance boundary conditions for imperfectly conducting surfaces," *Applied Science Research*, vol. 8, pp. 418-436, 1960.

[13] K. M. Mitzner, "An integral equation approach to scattering from a body of finite conductivity," *Radio Science*, vol. 2, pp. 1459-1470, 1967.
[14] E. Tuncer, B.-T. Lee, and D. P. Neikirk, "Interconnect Series Impedance Determination Using a Surface Ribbon Method," IEEE 3rd Topical Meeting on Electrical Performance of Electronic Packaging, Monterey, CA, Nov. 2-4, 1994, pp. 249-252.
[15] B.-T. Lee, E. Tuncer, and D. P. Neikirk, "Efficient 3-D Series Impedance Extraction using Effective Internal Impedance," IEEE 4th Topical Meeting on Electrical Performance of Electronic Packaging, Portland, OR, Oct. 2-4, 1995, pp. 220-222.
[16] B.-T. Lee and D. P. Neikirk, "Minimum Segmentation in the Surface Ribbon Method for Series Impedance Calculations of Microstrip Lines," IEEE 5th Topical Meeting on Electrical Performance of Electronic Packaging, Napa, CA, October 28-30, 1996, pp. 233-235.
[17] A. K. Agrawal, H. L. Price, and S. H. Gurbaxani, "Transient Response of Multiconductor Transmission Lines Excited by a Nonuniform Electromagnetic Field," *IEEE Transactions on Electromagnetic Compatibility*, vol. EMC-22, pp. 119-129, 1980.
[18] S. Ramo, J. R. Whinnery, and T. V. Duzer, *Fields and Waves in Communication Electronics*, 2nd ed. New York: Wiley, 1984.
[19] W. T. Weeks, L. L. Wu, M. F. McAllister, and A. Singh, "Resistive and inductive skin effect in rectangular conductors," *IBM Journal of Research and Development*, vol. 23, pp. 652-660, 1979.
[20] B.-T. Lee and D. P. Neikirk, "Minimum Segmentation in the Surface Ribbon Method for Series Impedance Calculations of Microstrip Lines," IEEE 5th Topical Meeting on Electrical Performance of Electronic Packaging, Napa, CA, October 28-30, 1996, pp. 233-235.
[21] M. Kamon, M. J. Tsuk, and J. White, "FASTHENRY: A Multipole-Accelerated 3-D Inductance Extraction Program," *IEEE Transactions on Microwave Theory and Techniques*, vol. 42, pp. 1750-1758, 1994.
[22] F. M. Tesche, "On the Inclusion of Loss in Time-Domain Solutions of Electromagnetic Interaction Problems," *IEEE Trans. on Electromagnetic Compatibility*, vol. 32, pp. 1-4, 1990.
[23] S. Kellali and B. Jecko, "Implementation of a Surface Impedance Formalism at Oblique Incidence in FDTD Method," *IEEE Trans. on Electromagnetic Compatibility*, vol. 35, pp. 347-355, 1993.
[24] J. G. Maloney and G. S. Smith, "The Use of Surface Impedance Concepts in the Finite-Difference Time-Domain Method," *IEEE Trans. on Antennas and Propagation*, vol. 40, pp. 38-48, 1992.
[25] K. S. Oh and J. E. Schutt-Aine, "An Efficient Implementation of Surface Impedance Boundary Conditions for the Finite-Difference Time-Domain Method," *IEEE Trans. on Antennas and Propagation*, vol. 43, pp. 660-666, 1995.
[26] E. Tuncer and D. P. Neikirk, "Efficient Calculation of Surface Impedance for Rectangular Conductors," *Electronics Letters*, vol. 29, pp. 2127-2128, 1993.
[27] S. Kim and D. P. Neikirk, "Compact Equivalent Circuit Model for the Skin Effect," IEEE International Microwave Symposium, Vol. 3, San Fransisco, CA, 1996, pp. 1815-1818.
[28] C. R. Paul, "Incorporation of Terminal Constraints in the FDTD Analysis of Transmission Lines," *IEEE Trans. on Electromagnetic Compatibility*, vol. 36, pp. 85-91, 1994.

EFFICIENT TIME DOMAIN BOUNDARY CONDITIONS FOR FINITE CONDUCTIVITY METALS

As clock speeds become faster and chips become more complex, it is more difficult to accurately predict delay and crosstalk in densely packed multi-conductor interconnects. The impact of frequency dependent inductance and resistance due to finite conductivity conductors on time domain waveforms has often been ignored or only poorly approximated even though this can cause overestimation of far-end crosstalk and underestimation of delay. To include frequency dependent effects accurately in time domain calculations, transformation using FFT is usually required. However, it is difficult to implement non-linear drivers using this method. In [3], a surface impedance boundary condition was applied directly to the time domain to solve radiation problems where high frequency approximation for surface impedance boundary condition is accurate enough. Here we show a new method for transmission line analysis where the boundary condition is represented directly in the time domain. Unlike other time domain simulation methods in which all the RLC parameters of the transmission lines must be provided a priori, in our model all required values are determined directly and simply from conductor geometry. The resulting frequency domain model is valid over a wide frequency range, and hence giving accurate time domain results. The method is also compatible with non-linear drivers and loads.

Application of impedance boundary condition in the time domain

Rapid calculation of interconnect series impedance in the frequency domain can be performed using an impedance boundary condition [2]. For a rectangular conductor cross section, the cross section is partitioned into two trapezoidal and triangular parts as shown in figure 2a; the "transverse impedance" of each part is used as an approximation of impedance boundary condition for the conductor [2]. To complete the problem, each transverse impedance is assigned to a corresponding surface ribbon and mutual inductances between these ribbons are calculated. The resulting two dimensional equation is

$$[Z_{eii}][I]+j\omega[L][I]=-\frac{\partial}{\partial z}[V]\ , \qquad (1)$$

where $[Z_{eii}]$ is a diagonal matrix of the effective internal impedances (EII) (representing the impedance boundary condition) and $[L]$ is a dense matrix of mutual inductances between ribbons.

To use this frequency domain concept in time domain analysis, the equivalent circuit shown in figure 2b is used to model each ribbon. This produces a rational function in the s-domain that is easily converted into time domain exponential functions. All values in this circuit model are determined directly from simple, closed form expressions depending on only the conductivity and geometry of the conductors [5, 6]. Transforming (1) into the time domain gives

$$[\zeta(t)]*\frac{\partial}{\partial t}[I]+[L]\frac{\partial}{\partial t}[I]=-\frac{\partial}{\partial z}[V]\ , \qquad (2)$$

where '*' represents convolution, $[\zeta(t)]$ is a sum of exponential functions obtained by converting the rational function in s-domain $[Z_{eii}/s]$, i.e.,

$$\frac{Z_{eii}}{s} = \frac{a_3 s^3 + a_2 s^2 + a_1 s + a_0}{s\left(b_3 s^3 + b_2 s^2 + b_1 s + b_0\right)} = \frac{k_1}{s} + \frac{k_2}{s+p_2} + \frac{k_3}{s+p_3} + \frac{k_4}{s+p_4} \quad . \qquad (3)$$

The rational function in (3) can be further reduced by using dominant pole approximation to reduce the computation time and memory usage.

The convolution appearing in (2) can be evaluated easily using a recursive relationship [7],

$$Y(n\Delta t) = ke^{p\Delta t} \cdot X(n\Delta t) = k\Delta t \cdot X(n\Delta t) + e^{p\Delta t} Y((n-1)\Delta t) \quad . \qquad (4)$$

Applying (3) to (2) yields

$$([k\Delta t] + [L])\frac{\partial}{\partial t}[I] + [V_{ds}] = [L']\frac{\partial}{\partial t}[I] + [V_{ds}] = -\frac{\partial}{\partial z}[V] \quad , \qquad (5)$$

where $[V_{ds}]$ is an extra voltage-dependent source added to the telegrapher's equation, depending on Δt and on the poles and residues of the equivalent circuit of the EII. Since Δt is usually very small, this voltage dependent source is mainly responsible for incorporating the current redistribution effects (i.e., the frequency dependent proximity and skin effects) in the time domain. Equation 4 is then solved along with the second telegrapher's equation for the shunt admittance (e.g., the capacitance) of the interconnect.

Method of characteristics

The method of characteristics was first developed to simulate a single lossless line [8], then later extended to multi-resistive lines [9]. Recently, it was further extended to non-uniform lossy line cases [10], where frequency dependent series impedance is calculated using FFT. Here, for simplicity, a homogeneous medium with $[G]$=0 is assumed. More general cases are well demonstrated in [10]. From equation 4 and the corresponding admittance equation,

$$d([V] \pm [R][I])/dt = -[V_{ds}] \cdot v_p \quad , \qquad (6)$$

where $[R] = v_p[L']$, v_p is propagation velocity and +/- represent incident and reflected waves, respectively. To capture the distributed resistive effects intermediate segmentation is required, then equation 8 becomes

$$\{[V] + [R][I]\}(x_{k+1}, t_{n+1}) = \{[V] + [R][I] - \Delta t \cdot v_p[V_{ds}]\}(x_k, t_n) \,, \qquad (7a)$$

for the incident wave, and for the reflected wave

$$\{[V] - [R][I]\}(x_{k-1}, t_{n+1}) = \{[V] - [R][I] + \Delta t \cdot v_p[V_{ds}]\}(x_k, t_n) \quad . \qquad (7b)$$

The equivalent model is shown in figure 3; comparing to the model shown in [11], the resistance is replaced with a new voltage-dependent source to capture frequency dependent effects. To simulate rectangular conductors, each conductor is divided into four parts as shown in figure 2a, then each part is represented with its equivalent circuit, and finally four parts are connected in parallel.

Results and conclusions

Figure 4 shows simulation results obtained using the new method introduced in this paper, as well as illustrated the errors resulting from failure to properly include the time/frequency dependencies of both resistance and inductance. Excellent agreement is shown compared to FFT method using a full dispersion curve, while the CPU time required for this method (7.6 seconds) is much less than the FFT method (283 seconds). In conclusion, this paper demonstrates that the dc to skin effect frequency variation of series impedance can be directly and accurately included in the time domain, with all needed values can be easily determined directly from conductor geometry, while maintaining high numerical efficiency.

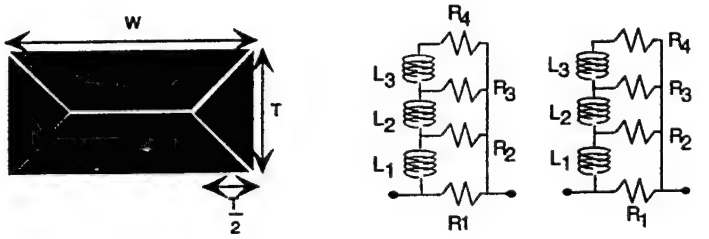

Figure 2) (a) Segmentation scheme for rectangular bar to approximate surface impedance. (b) Equivalent circuit model for approximated surface impedance.

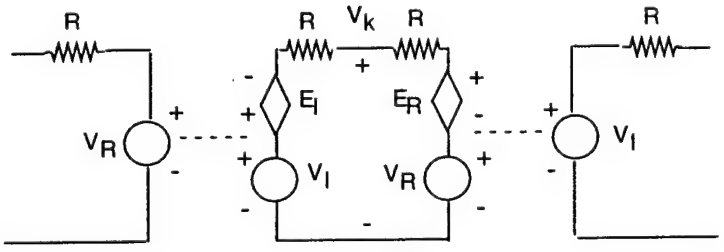

Figure 3) Equivalent model for method of characteristics. E_R and E_I are voltage dependent sources of reflected and incident waves respectively and appear in second part of right hand side of the equation 8a and 8b, respectively.

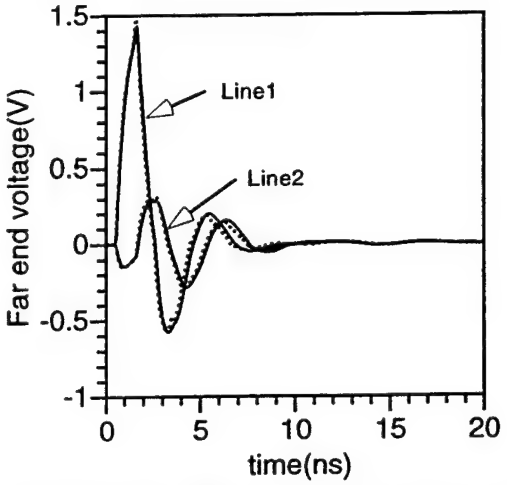

(a) far end waveform at line 1 and 2; solid line: FFT result, dotted line: new method described here.

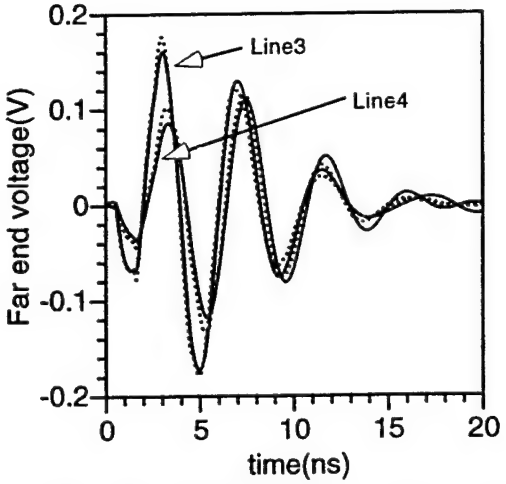

(b) far end waveform at line 3 and 4; solid line: FFT result, dotted line: new method described here.

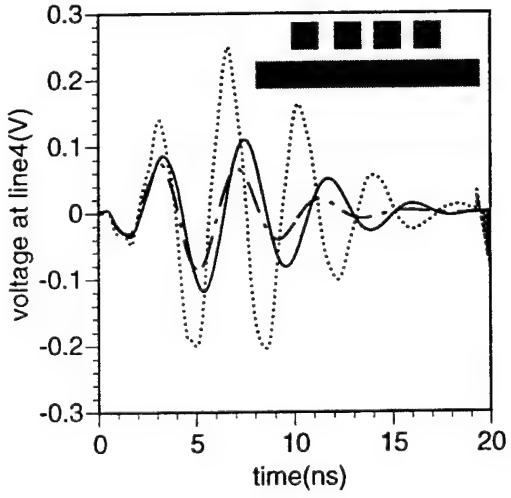

(c) far end voltage waveform at line 4: errors induced by failure to correctly include both resistance and inductance frequency dependencies: Solid line: FFT using full dispersion curve; dotted line: constant R-L-C transmission line analysis; dashed-dotted line: Star-Hspice® 97.2 using W Element where one high frequency resistance value must be calculated using some other method (here, the surface ribbon method was used [2]).

Figure 4) Simulation results for 4 lines above a ground plane. Conductor geometry: width & thickness = 20 μm, separation between conductors = 10 μm, signal conductors 10 μm above ground plane, ground plane 20 μm thick, 170 μm wide, line length = 0.1 m. Input wave form applied to line 1 only: 1V trapezoidal wave with rise, fall time = 0.1 ns, duration = 1 ns; source resistance = 5 Ω, terminated with 10 pF capacitance.

References

[1] A. Deutsch, et al., "The Importance of Inductance and Inductive Coupling for On-chip Wiring," IEEE 6th Topical Meeting on Electrical Performance of Electronic Packaging, San Jose, CA, October 27-29, 1997, pp. 53-56.

[2] E. Tuncer, et al., "Interconnect Series Impedance Determination Using Surface Ribbon Method," 3rd topical meeting on Electrical Performance of Electronic Packaging, Monterey, CA, 1994, pp. 250-252.

[3] J. G. Maloney and G. S. Smith, "The Use of Surface Impedance Concepts in the Finite-Difference Time-Domain Method," *IEEE Transactions on Antennas and Propagation*, vol. 40, pp. 38-48, 1992.

[4] B.-T. Lee and D. P. Neikirk, "Minimum Segmentation in the Surface Ribbon Method for Series Impedance Calculations of Microstrip Lines," IEEE 4th topical meeting on Electric Performance of Electronic Packaging, Portland, OR, 1996, pp. 220-222.

[5] S. Kim and D. Neikirk, "Compact Equivalent Circuit Modeling for the Skin Effect," IEEE International Microwave Symposium, San Francisco, CA, 1996, pp. 1815-1818.

[6] S. Kim and D. P. Neikirk, "FDTD Time Domain Multiconductor Transmission Line Analysis Using Effective Internal Impedance," IEEE 6th topical meeting on Electrical Performance of Electronic Packaging, San Jose, CA, 1997,

[7] S. Kellali, et al., "Implementation of a Surface Impedance Formalism at Oblique Incidence in FDTD Method," *IEEE Transactions on Electromagnetic Compatibility*, vol. 35, pp. 347-355, 1993.

[8] F. H. Branin, "Transient Analysis of Lossless Line Systems," *Proceedings of IEEE*, vol. 55, pp. 2012, 1967.

[9] C. W. Ho, "Theory and Computer-aided Analysis of Lossless Transmission Lines," *IBM J. Res. Develop.*, vol. 17, pp. 249-255, 1973.

[10] J.-F. Mao and Z.-F. Li, "Analysis of the Time Response of Multiconductor Transmission Lines with Frequency-Dependent Losses by the Method of Convolution Characteristics," *IEEE Transactions on Microwave Theory and Techniques*, vol. 40, pp. 637-644, 1992.

[11] A. J. Gruodis, "Transient Analysis of Uniform Resistive Transmission Lines in a Homogeneous Medium," *IBM J. Res. Develop.*, vol. 23, pp. 675-681, 1979.

HP-FINITE ELEMENTS APPLIED TO ELECTROMAGNETIC PROBLEMS

Another important advance in the area of computational electromagnetics for application to mixed signal simulation has been in the area the finite element method (FEM). A new hp-adaptive technique has recently been validated that allows the local variation of both the element size (h) and the order of approximation (p). This approach has the advantage that complex structures should be easily simulated. The formulation has been demonstrated to allow discontinuous changes in material properties (such as the change from a dielectric to a metal), to be stable, and to easily handle curvilinear geometries. Extensive numerical testing is still required in this area.

Numerical schemes based on nodal finite elements have been successfully applied to many electromagnetic problems formulated in terms of potentials. Unfortunately, this methodology frequently fails if extended directly to the field equations, and new families of so called "edge-based" elements have been proposed. However, in the low frequency range, the traditional formulation becomes unstable even with the "edge-based" elements and can lead to spurious solutions. In this thesis, we present a general hp-adaptive methodology, free of spurious solutions over the entire range of physically relevant frequencies for steady-state Maxwell's equations in interior domains.

We design our family of H(curl)-conforming hp-edge elements in the context of a model problem with sources. These elements generalize the well-known edge elements of Nedelec [4, 5]. We confirm that finite element spaces built on our elements ensure discrete compactness and commutativity of de Rham complex, two fundamental properties necessary for stability and convergence of mixed methods for Maxwell's equations. Analytical results suggest that the method remains stable even at very low frequencies.

Following the logic applied to the model problem, we develop a new formulation for the full-wave analysis of waveguides. Using the discrete compactness, we prove that this formulation leads to numerical approximations which define a family of collectively compact operators. Relying on the result by Chatelin [1], we show that these operators converge not only pointwise but also in the operator norm. To the best of our knowledge, this result as well as a study on spectral convergence at a given frequency, has never been published in the literature.

In our study on spectral convergence, we relate the discrepancy between exact and numerical eigenvalues to the interpolation error. The actual convergence rate estimates are for shape-regular meshes with element-dependent order of polynomial approximation p which remains uniformly bounded from above. The convergence estimates are derived for non-conducting Lipschitz polygons with piece-wise continuous e, m, and for polygons with slits provided e, m, are constants. We stress that our approach is general and applies to any family of vector elements which satisfy the discrete compactness, approximability and some compatibility properties. For example, our analysis covers standard Nedelec elements of [4, 5]. Based on the new formulation, a finite element code for the full-wave analysis of waveguides has been written. This Fortran 90 code is built on top of the 2Dhp90_EM package for electromagnetics [6] which supports the new hp-edge finite elements.

Performed numerical experiments fully confirm our analytical convergence estimates obtained for affine non-conducting domains, Figure 5 and Figure 6, and suggest that these estimates remain valid for domains with nonzero conductivity and curved boundaries, Figure 7 and Figure 8.
We show that the code correctly captures and tracks the development of a complex mode in a shielded lossless microstrip in Figure 1. The dispersion curves in Figure 2 for some representative modes, including a complex mode, are produced using non-uniform hp-meshes with two levels of h-refinement performed at the tip. Scalar hp-quads of order ps = 2, 3, 4 are linked with compatible hp-edge elements.

To test the method on structures of practical interest, we perform the full wave analysis of microstrip depicted in Figure 3. Dimensionless numerical frequency corresponding to the domain used to compute attenuation constants of this microstrip can drop below 10-6 on the global level, and below 10-8 on the element level. The obtained results show that the formulation is indeed stable as w —+ 0. In Figure 4, we observe that the FE-method based on our formulation and implemented using the hp-elements yields the attenuation curve marked "FE" which is in a good agreement with the curve computed by means of a conformal mapping technique taken from [3].

We believe that our work has prepared a solid foundation for a fully automatic hp-adaptive finite element code for full-wave analysis of waveguides. For a detailed discussion on the subject, we refer to [7].

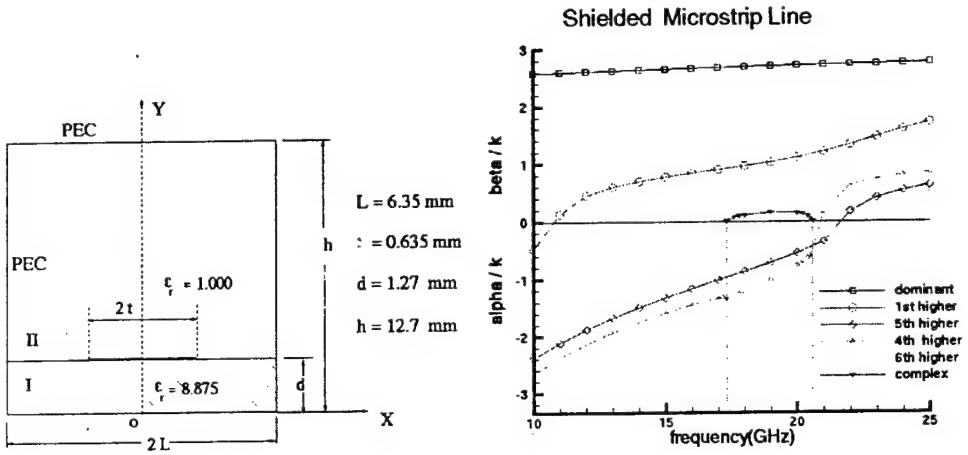

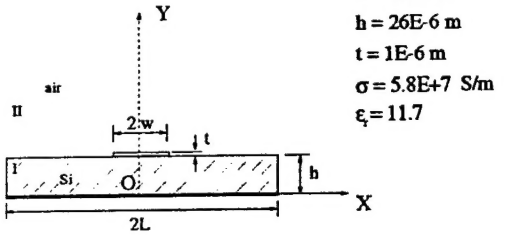

L = 250E-6 m
w = 10E-6 m
h = 26E-6 m
t = 1E-6 m
σ = 5.8E+7 S/m
ε_r = 11.7

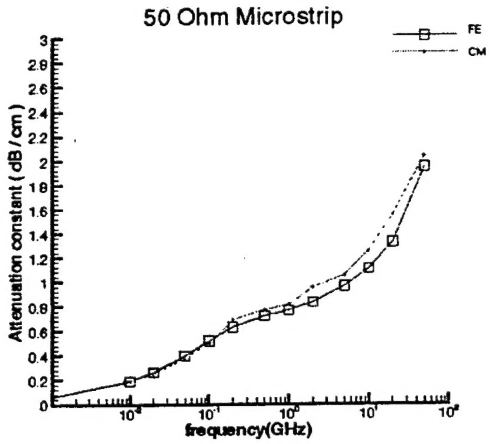

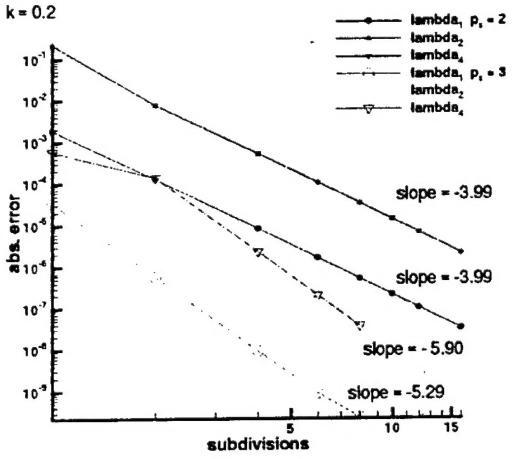

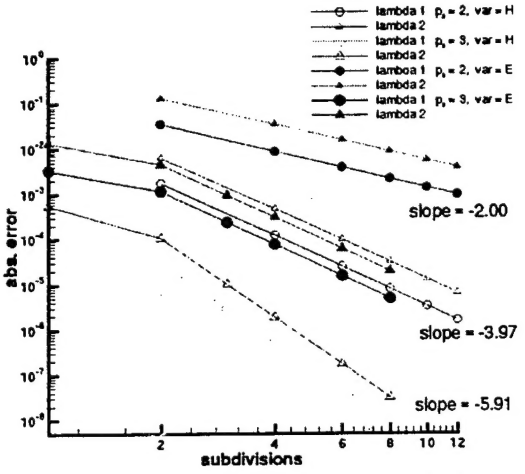

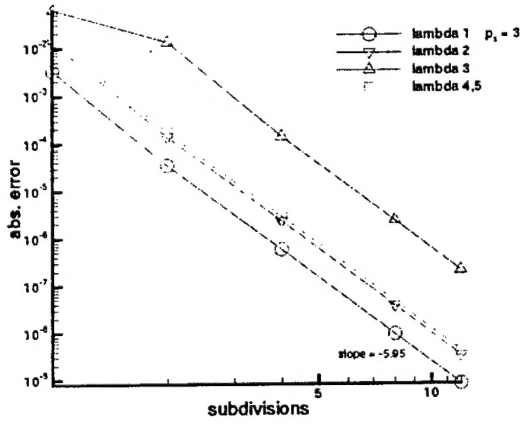

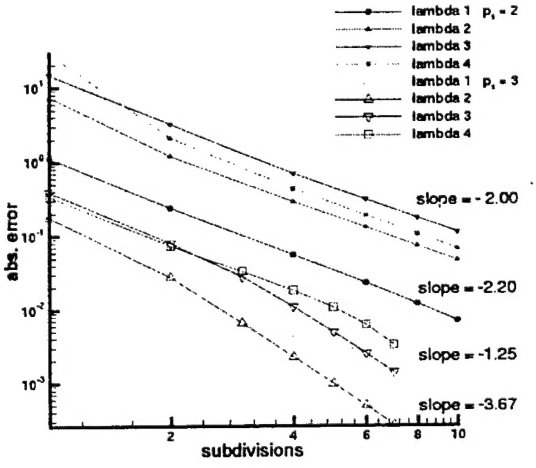

References

[1] F. Chatelin Spectral Approximations of Linear operators , Academic Press, NY, 19 83.

[2] L. Demkowicz, L. Vardapetyan , "Modeling of Electromagnetic Absoption/Scattering Problems Using hp-adaptive Finite Elements", Computer Methods in Applied Mechanics and Engineering, 152, 1-2, 103-124, 1998.

[3] B.-T., Lee, Efficient Series Impedance Extraction Using Effective Internal Impedance. Ph.D. thesis, Graduate School of The University of Texas at Austin, August 1996.

[4] J.C. Nedelec, "Mixed Finite Elements in R3" Numerische Mathematik, 35, 315-341. 1980.

[5] J.C. Nedelec, "A New Family of Mixed Finite Elements in~3". Numerische Mathematik, 50, 57-81. 1986.

[6] W. Rachowicz. L. Demkowicz, "A Two-Dimensional hp—Adaptive FE Package for Electro magnetics". TICAM Report 98-15, July 1998.

[7] L. Vardapetyan, hp-Adaptive Finite Element Method for Electromagnetics with Applications to Waveguiding Structures, Ph.D. thesis, Graduate School of The University of Texas at~ Austin, December 1999.

EXPERIMENTAL MEASUREMENTS ON A PROTOTYPICAL PERSONAL COMMUNICATIONS SERVICES (PCS) SYSTEM

Our research activities in this area have been focused on building RF transceivers and baseband circuits for a handset testbed at 1.8GHz, the personal communication services(PCS) band. One important objective of this effort is to fully understand how the PCB layout, chip placement and packaging affect the overall wireless system specifications. This knowledge will help us to properly design multi-chip module (MCM) package for wireless communication systems.

The stability of frequency synthesizers, realized by phase locked loop, is critically important to the quality of wireless communications. If they lose lock even for a short period of time, they can cause significant problems with the modulation and demodulation. In our experiments, we found that the phase locked loop (PLL) was very sensitive to the interference from the power supply, sudden changes of impedance, and interference from power amplifiers. The RF transceivers we built were for the time-division-duplex (TDD) applications, in which the transceivers transmit in a 5ms slot and receive in another 5ms slot. During the transition period, the transmitter mixer is turned off and on to minimize the RF coupling between the transmit and receive parts. However, this causes sudden changes of the load impedance to the PLL and unlocks the PLL. Although the PLL can recover from this sudden change eventually, it may cause significant distortion or phase noise to the beginning part of the signal. Hence, in a mixed signal package, it is better to build some driver on the die or inside the package to avoid the detrimental effect due to the change of impedance. Also, the PLL must not share the same power supply as the power amplifier since the supply current surges after the power amplifier is turned on and dips if the power amplifier is turned off. This is another source for the PLL to lose lock for a short period of time. Hence, in the MCM package, we should have a different VCC pin just for the PLL power supply. Another source of the PLL problem is due to the leakage power from the power amplifier. If we lay the RF board on a table, there is no problem. However, once we place another baseband board on the top of that, the leaked power will be reflected from the baseband board and coupled to the PLL. If we wish to package a PLL in the same MCM package as the power amplifier, care must be taken to isolate the PLL from the power amplifier.

On the baseband board, we used the Motorola digital signal processor MC56167 as a vocoder DSP. There are several delicate design issues and test issues we would like to address. This part is a mixed signal part. Although the analog ground and digital ground are separate in the chipset, care must be taken to eliminate the digital noise in the analog codec part. We have tried numerous PCB layouts and still could not eliminate the digital background noise. Later we managed to minimize the noise by balance the load of the DSP. In our vocoder, the encoding part takes much more time than the decoder part. Thus, the DSP may be busy for some time and idle for some time. In this case, the noise from the DSP shows some periodical pattern and is more easily sensed by a human ear. We managed to change the DSP structure and made it busy all the time. This makes the noise white and not so sensible. Therefore, for testing the digital interference to the analog circuits in a mixed signal package, we should try to have several test patterns with different loading to assess the digital interference to the analog part.

SUMMARY

In summary, we have extended our ability to efficiently simulate the behavior of realistic interconnects that make use of finite conductivity metals. In particular, we have developed and tested:

- a fundamental electromagnetic formulation of the effective internal impedance boundary condition for finite conductivity metals.
- an extremely efficient multi-conductor simulation program using the surface ribbon method for interconnect series impedance calculations.
- initial computational electromagnetics code for FEM simulations.
- experimental work on mixed signal PCS prototypes to investigate analog system corruption due to cross talk and power supply noise.

PUBLICATIONS SUPPORTED IN WHOLE OR IN PART BY THIS GRANT:

B.-T. Lee and D. P. Neikirk, "Minimum Segmentation in the Surface Ribbon Method for Series Impedance Calculations of Microstrip Lines," *IEEE 5th Topical Meeting on Electrical Performance of Electronic Packaging*, Napa, CA, October 28-30, 1996, pp. 233-235.

Beom-Taek Lee, Sangwoo Kim, Emre Tuncer, and Dean P. Neikirk, "Effective Internal Impedance Method for Series Impedance Calculations of Lossy Transmission Lines: Comparison to Standard Impedance Boundary Condition," submitted to: IEEE Transactions on Microwave Theory and Techniques, June 1997.

Sangwoo Kim and Dean P. Neikirk, "Time Domain Multiconductor Transmission Line Analysis Using Effective Internal Impedance," *IEEE 6th Topical Meeting on Electrical Performance of Electronic Packaging*, San Jose, CA, October 27 - 29, 1997, pp 255-258.

S.-J. Yoo, R. Friar, and D. P. Neikirk, "Analytic modeling of monolithic inductors on semiconductor substrates," IEEE Topical Meeting on Electrical Performance of Electronic Packaging, , Oct 26-28, 1998, pp. 219-222.

Beom-Taek Lee, PhD dissertation title: "Efficient Series Impedance Extraction Using Effective Internal Impedance," Aug. 1996.

Sangwoo Kim, dissertation title: "Multiconductor Transmission Line Analysis Using Surface Ribbon Method," Aug. 1999.